Experimental Investigation of Heat Transfer Rates in Rocket Thrust Chambers

ARVEL B. WITTE[1] AND EDWARD Y. HARPER[2]
Jet Propulsion Laboratory, California Institute of Technology, Pasadena, Calif.

An experimental investigation was conducted to determine local values of heat flux in rocket engine thrust chambers that incorporated convergent-divergent nozzles of two different geometries. The largest nozzle expansion-area ratio investigated was 20 to 1. Chamber pressures ranged from 100 to 300 psia at thrust levels between 1000 and 5000 lbf. The propellants used were nitrogen tetroxide (N_2O_4) and hydrazine (N_2H_4) at a nominal mixture ratio of 1.0. Effects on Stanton number are shown for Reynolds number changes caused by varying chamber pressure and by variations in diameter along the nozzles.

Nomenclature

b = radius of wall curvature, in.
C = constant
c_p = specific heat at constant pressure, Btu/lbm-°R
$\bar{c}_p$ = average specific heat across boundary layer (including effects of chemical reaction), Btu/lbm-°R
c^* = characteristic velocity $(p_c A^* g_c)/\dot{m}$, fps
D = diameter, in.
g_c = gravitational constant, 32.2 lbm-ft/lbf-sec²
h_i = enthalpy convective heat transfer coefficient h_T/c_p, lbm/in.²-sec
h_T = temperature convective heat transfer coefficient, Btu/in.²-sec-°R
i = enthalpy, Btu/lbm
l^* = axial distance from nozzle entrance to nozzle throat, in.
l_x = axial distance from nozzle entrance to nozzle exit, in.
L^* = characteristic combustion-chamber length, in.
p = pressure, psia
Pr = Prandtl number, dimensionless
q = heat flux, Btu/in.²-sec
r = mixture ratio, $\dot{m}_{\text{oxidizer}}/\dot{m}_{\text{fuel}}$
R = radial coordinate, in.
Re_D = Reynolds number based on diameter, dimensionless
St = Stanton number, dimensionless
T = temperature, °R
u = velocity, fps
x = axial distance coordinate, in.
γ = ratio of specific heats
Δp = pressure difference, psi
ϵ_c = nozzle contraction-area ratio
ϵ_e = nozzle expansion-area ratio
μ = viscosity, lbm/in.-sec
ρ = density, lbm/ft³
σ = see Appendix

Superscripts and subscripts

c = constant-diameter combustion chamber
D = diameter
e = experimental
E = freestream edge of boundary layer
i = enthalpy
IO = injector orifice
max = maximum
p = predicted
ref = reference temperature
s = static
SP = splash plate
T = temperature
w = wall
1-D = one-dimensional
0 = stagnation
* = nozzle throat
′ = reactive condition

A KNOWLEDGE of the distribution of heat flux or heat transfer coefficient is mandatory for the proper design of rocket engine thrust chambers; consequently, some means of predicting these quantities must be made available. It is the objective of this experimental study to contribute to the information, which hopefully will lead to an eventual understanding of the basic heat transfer phenomena that occur in a rocket engine.

It is clearly evident that not only mass flow rate but also several other complex interacting phenomena, such as radiation, chemical reaction, turbulence, secondary flows, and other flow nonuniformities, must influence the net heat transfer to the wall of a rocket motor. Nevertheless, there is a compelling desire, because of the inability to describe the complicating phenomena, to attempt to relate at least the axial variation of heat flux to the mean mass flow rate at each axial station. Surprising, perhaps, is the fact that some success has been achieved with such a correlation, e.g., the results presented in Refs. 1 and 2. The specific basis on which the mean-flow-related convective heat transfer is predicted is probably not very important because the differences in various experimental results due to variable operating conditions tend to exceed the differences in these specific predictions.

One model on which such predictions have been made is based on the fairly sound assumption that the convective heat transfer in a rocket nozzle is related to the growth of turbulent velocity and temperature boundary layers (1).[3] A solution for the development of these boundary layers was found through the use of the integral momentum and integral energy equations, which take into account the pressure gradient. The resulting boundary layer thicknesses had to be related to the heat transfer, however. Because of a lack of knowledge of the effects of pressure gradient, it was assumed that such effects were confined to the development of the boundary layer, and that the usual flat-plate, skin-friction law (based on the local boundary layer thickness) and a slightly modified flat-plate Reynolds analogy would give reasonable results. Somewhat later, in order to avoid lengthy boundary layer calculations, a simple closed-form approximation to these results was developed for a restricted class of nozzle configurations (2) by using the local nozzle diameter as a nondimensionalizing length parameter. The choice of diameter was quite appropriate, since the boundary layer thickness varies in fairly systematic relation to the local diameter throughout a nozzle. The resulting equation, ex-

Received by ARS July 5, 1962; revision received September 19, 1962.

[1] Research Engineer, Heat Transfer and Fluid Dynamics Group, Propulsion Research Section.

[2] Presently with Lockheed Missiles and Space Company, Sunnyvale, Calif.

[3] Numbers in parentheses indicate References at end of paper.

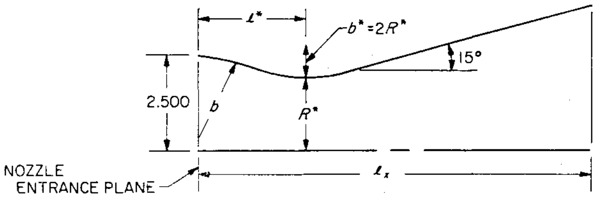

ϵ_c	b	L^*	R^*	L_x
1.64 to 1	3.90	2.880	1.950	10.384
2.5 to 1	3.160	3.411	1.580	7.230
4 to 1	2.500	3.312	1.250	7.050
8 to 1	1.42	3.66	0.884	7.50

Fig. 1 Nozzle configurations

pressed for convenience in terms of rocket engine operating parameters, appears as Eq. [A1] in the Appendix. When reduced to its equivalent nondimensional form using conventional nondimensional parameters, the equation is

$$St\, Pr^{0.6} = C\, Re_D^{-0.2} \tag{1}$$

That Eq. [1] is in exactly the same form as the familiar pipe-flow heat transfer correlation equation is not surprising inasmuch as 1) direct use is made of the same basic skin-friction law (Blasius) and of essentially the same relation between skin friction and heat transfer (slightly modified Reynolds analogy), and 2) local diameter is used as the nondimensionalizing parameter. Obviously, to account for the more drastic effects of thin boundary layers at a nozzle entrance or for radical changes in nozzle configurations, the simple closed-form approximation cannot work, and one must resort to solving for the actual boundary layer development. In many cases, however, it would appear that the effects of axial boundary layer variations on nozzle convective heat transfer are overshadowed by axial variations in mean mass flux. It is not clear even now, however, that the influence of axial variations of mean mass flux (or equivalently, pressure gradient) is properly accounted for in the assumed skin-friction law and analogy. Certainly, there is little fundamental information available which would either validate the approach or suggest an alternative. The results presented herein, although influenced by combustion effects, suggest that the effects of pressure gradient require further study.

The purpose of this investigation was to extend the initial nozzle heat transfer results reported in Refs. 3 and 4, with special attention to important areas of general interest not covered in those references. In particular, additional information was desired concerning 1) values of heat flux at intermediate contraction-area ratios and at supersonic area ratios between 4 to 1 and 20 to 1, 2) local rather than semilocal values of heat flux, and 3) a comparison of the results of 1 and 2 with Eq. [A1]. In addition, it was considered desirable to correlate the results of the two investigations in nondimensional form in order to clarify the relationship between chamber pressure and convective nozzle heat transfer alluded to in Refs. 3 and 4.

Heat fluxes were determined experimentally in a 2.5-to-1 contraction-area ratio water-cooled nozzle by calorimetry and in a 1.64-to-1 contraction-area ratio uncooled nozzle by transient wall-temperature measurements. Thrust ranged from 1000 to 5000 lbf as chamber pressure was varied between 100 and 300 psia. A splash-plate (Enzian) type of injector was used with nitrogen tetroxide (N_2O_4) and hydrazine (N_2H_4) as propellants operating at a mixture ratio of 1.0. The 2.5-to-1 nozzle was constructed with axially short, circumferential cooling passages that provided semilocal heat-flux results determined by calorimetry. It had an expansion-area ratio of 20 to 1. The 1.64-to-1 nozzle was instrumented with wall thermocouples that provided boundary conditions used in solving the transient heat conduction equation for radial temperature distribution as a function of time. It had an expansion-area ratio of 3.78 to 1.

For the present investigation, radiant heat exchange between the products of combustion and the wall is estimated to be of an order of magnitude less than that due to convection; hence, radiation effects are neglected in the predicted values. The experimental measurements, however, include both effects, since no effort was made to distinguish between them.

Experimental Apparatus

A nitrogen-pressurized bipropellant flow system, the thrust stand on which the engine was mounted, and the electrical and pneumatic system with which the entire system was controlled and performance was measured (described in detail in Refs. 3 and 4) were used in conducting all tests. Several systems changes that are mentioned here briefly were made subsequent to the tests reported in Refs. 3 and 4. Propellant flow rates were controlled by cavitating venturis and measured with turbine flow meters. Two Photocon pressure transducers were installed flush with the inner surface of the chamber in order to measure the combustion pressure oscillations. A digital recording system was used in conjunction with the standard recording instrumentation.

Each thrust chamber consisted of an injector, a 5.0-in. constant-diameter combustion chamber, and a convergent-divergent nozzle. Changes in L^* were made by changing combustion chamber length. Nozzle geometries are given in Fig. 1. The tests were made with the eight-orifice pair splash-plate (Enzian) injector described in Refs. 3 and 4. Both uncooled and water-cooled chambers and nozzles were used.

A 1.64-to-1 contraction-area ratio,[4] uncooled, heat-sink type of nozzle rated at 5000-lb thrust at 300-psia chamber pressure was fabricated from type 1020 steel. This nozzle had the same inner contour as the 1.64-to-1 water-cooled nozzle described in Refs. 3 and 4. Two chromel-alumel wall thermocouples were installed on a line perpendicular to the gas-side surface at each of 17 positions in the nozzle. Ref. 7 describes in detail the fabrication and installation of the thermocouples.

The 2.5-to-1 nozzle nominally rated at 3300-lb thrust at 300-psia chamber pressure had an expansion-area ratio of 2.5 to 1. This nozzle employed axially short, circumferential coolant passages formed by a 0.075-in.-thick copper liner with integral stiffening rings and a polyester plastic outer casing similar to the plastic-cased 1.64-to-1 nozzle described in Ref. 3. Steady-state semilocal heat transfer rates were determined by a calorimetric method described in the next section. A water-cooled conical extension was attached to the exit end of this nozzle during the test program, which provided an expansion-area ratio of 20 to 1. This extension had a polyester outer casing and a 0.050-in.-thick type 347 stainless-steel liner and was similar in construction to the 2.5-to-1 nozzle. Steady-state semilocal heat transfer rates were determined by calorimetry.

A straight constant-diameter diffuser was used to permit sea-level testing of this nozzle at a chamber pressure near 300 psia. The diffuser had an L/D of 10 and an inside diameter of 13 in. Its design was based on considerations given in Ref. 6.

Heat-Flux Measurements

The two thermocouples in each plug of the uncooled nozzle provided the two temperature-time boundary conditions

[4] Henceforth, the phrase "contraction-area ratio" will be implied for nozzle designation.

used in solving the variable-property one-dimensional heat conduction equation in cylindrical coordinates for the wall temperature distribution as a function of time and radial distance. The heat conduction equation was written as a finite-difference equation and solved by numerical methods on an IBM 7090 computer. Ideally, the inner boundary condition would have been located at the gas-side surface so that Fourier's equation could have been evaluated directly for the heat flux. However, the thermocouple plug used an imbedded thermocouple that was nominally 0.020 in. from the gas-side wall surface. A fifth-order polynomial that fitted the temperature distribution between thermocouple boundary conditions was extrapolated to the gas-side wall where Fourier's equation was evaluated for the wall heat flux.

Fig. 2 shows a typical variation of experimental heat flux with wall temperature for a transient thermocouple plug in the uncooled nozzle. The severe oscillations that appear during the first 0.8 sec for the eight lowest wall temperature points are the combined effect of the combustion starting transient, the initial poor fit, and the consequent inaccurate extrapolation of the temperature distribution to the surface. All computer results taken from the region in which oscillations occurred were obtained by linear extrapolation from the region in which the oscillations were not pronounced.

Ref. 7 includes an analytical and experimental investigation of the transient wall temperature measurement technique for deducing heat flux in rocket engines. Included in Ref. 7 is the computer program, a study of computer response to various time and radial increments, as well as known temperature inputs and thermocouple positions.

Steady-state semilocal heat transfer rates were determined by calorimetry in circumferential, short axial coolant passages in the 2.5-to-1 nozzle, chamber, and water-cooled extension. Water flow rates and temperature rises were measured by cavitating venturis and chromel-constantan thermocouples, respectively. Steady values of thermocouple temperature were observed within 4 sec after ignition. Since the duration of all calorimetric tests was between 7 and 15 sec, all calorimetric heat fluxes reported were considered to be steady-state values. Heat fluxes were calculated by the product of water flow rate, temperature rise, and specific heat, divided by the heat transfer surface area.

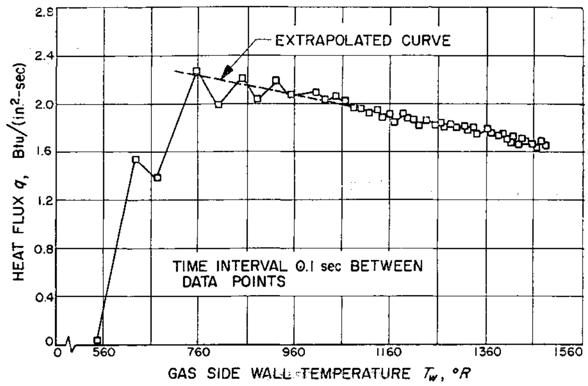

Fig. 2 Heat flux as a function of gas-side wall temperature for the uncooled 1.64-to-1 nozzle

Experimental Results

Performance

Characteristic velocity c^*, an important engine performance parameter used in nozzle heat transfer calculations, was determined for each test from measurements of propellant flow rate and chamber pressure. Static-pressure measurements made at the entrance to the nozzle were converted to stagnation values using $\gamma = 1.22$ and the subsonic Mach number corresponding to the nozzle contraction-area ratio. The experimental range of chamber pressure, characteristic velocity, and mixture ratio is shown in Table 1 for each test series. Experimental values of c^* for the eight-orifice pair splash-plate injector ranged between 88.9 and 94.5% of the theoretical c^*, which is 5800 fps at $r = 1.0$ (8). The higher values of c^* generally occurred at the higher L^* values. Nearly identical results were observed also for similar tests in Refs. 3 and 4. Mixture ratio was maintained at $1.00 \pm 3\%$ for all tests. No severe combustion instability was observed on the Photocon pressure-transducer records.

The experimental results of this investigation are presented in two fundamentally different ways. First, the axial distribution of heat flux for a representative number of tests covering the chamber pressure range for both the 1.64-to-1 and 2.5-to-1 nozzle is shown to permit full visualization of the trends and repeatability of the results. Second, all the results are compared on Stanton number-Reynolds number curves as a first step in limited generalization of the results of several thrust chamber configurations. Comparisons are also made between the experimental results and the method of predicting heat transfer coefficients in rocket nozzles by use of Eq. [A1]. Calculations of enthalpy heat transfer coefficient, Reynolds number, and Stanton number are included in the Appendix.

Figs. 3 and 4 show the axial distribution of heat flux obtained by the transient technique for the uncooled 1.64-to-1 nozzle at low and intermediate chamber pressures for four "A" series tests indicated in Table 1. Also shown in Figs. 3 and 4 are the values of experimental to predicted (Eq. [A3] enthalpy heat transfer coefficient ratio, h_{i_e}/h_{i_p}, vs length. The average "stepwise" values of heat flux included in these figures are results obtained with the water-cooled nozzle that had the same inner contour. The uncooled nozzle data are at the same wall temperature attained during the cooled tests. The heat flux calculated by use of Eq. [A1], based on the experimental c^* and p_c for the uncooled-nozzle tests, is shown also. Comparison of the scatter in the uncooled heat-flux results of Figs. 3 and 4 indicates that more scatter exists at higher chamber pressure. This is believed to be due, at least in part, to the faster wall temperature rise at higher pressure which provides fewer temperature-time data points for the calculation of heat flux. Some of the thermocouples were damaged during the tests; the results obtained from these are not shown.

It is believed that the differences between the uncooled and water-cooled nozzle heat fluxes in the contraction and throat regions are due in part to differences in the gas flow from test to test caused by the combustion process. Differences may arise also between the uncooled and water-cooled nozzle results, because point values of heat flux are obtained in the former case, whereas semilocal, circumferentially averaged values of heat flux are obtained in the latter. The results of both the uncooled and water-cooled nozzles indicate trends similar to those observed and reported in Refs. 3 and 4.

The good agreement of the uncooled and water-cooled nozzle results in the expansion region, where circumferential variations of heat flux are believed to be very small, indicates that the transient wall-thermocouple measurement technique of determining local heat flux is valid.

Figs. 5–7 show the axial distribution of semilocal heat flux obtained by calorimetry with the 2.5-to-1 water-cooled nozzle for five tests ranging between 100- and 300-psia chamber pressure. As before, the lower half of each figure shows the enthalpy heat transfer coefficient ratio h_{i_e}/h_{i_p}.

This ratio has not been calculated in the combustion-chamber region, where the application of the uniform-flow convection heat transfer equation (Eq. [A1]) has the least rational basis. Only the higher-performance test-series results of 36-in. L^*, rather than the lower-performance results of 18-in. L^*, are shown. The effect of increasing L^* from 18 to 36 in. on nozzle heat flux at 100- and 150-psia chamber pressure was to reduce the magnitude of the heat flux level by approximately 8%. This result, however, was not observed conclusively at the higher chamber pressures. Eq. [A1] yields an increase of heat flux with the larger L^*, solely because of the higher c^* obtained at that condition. The opposing trends of predicted and experimental values of heat flux lead to the conclusion that proximity to regions of strong flow recirculation and turbulence promotes deviations from the anticipated convection heat transfer rates. In addition, it is believed that the thinner boundary layer resulting from the shorter chamber of 18-in. L^* contributes to the observed trends.

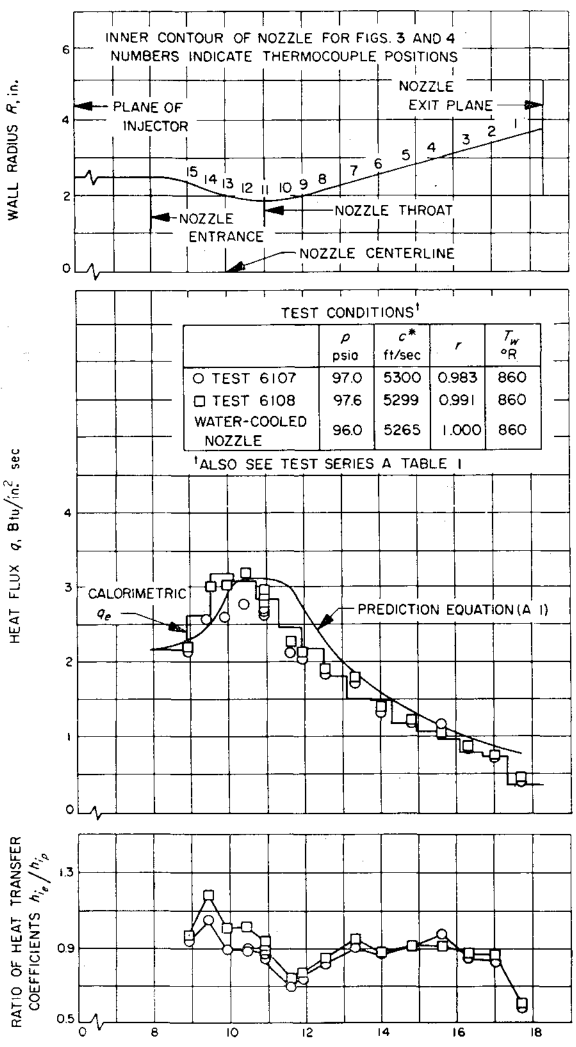

Fig. 3 Nozzle contour, heat flux, and enthalpy heat transfer coefficient ratio as a function of axial distance for the 1.64-to-1 nozzle at low chamber pressures

The comparatively high values of heat flux observed at a few locations in the expansion regions (Figs. 6 and 7) were the result of partial restrictions in cavitating venturis caused by flakes of rust which occasionally entered the system.

For the results shown in Figs. 6 and 7, the 20-to-1 water-cooled extension was attached to the straight constant-diameter diffuser, which maintained an exit pressure p_x of approximately 4 psia. Calculations using the flow-separation data presented in Ref. 9 indicated that separation occurred at or very near the coolant passage adjacent to the diffuser in tests 6141 and 6142 of Fig. 6. It is believed that the extended nozzle flowed full in test 6143 of Fig. 7.

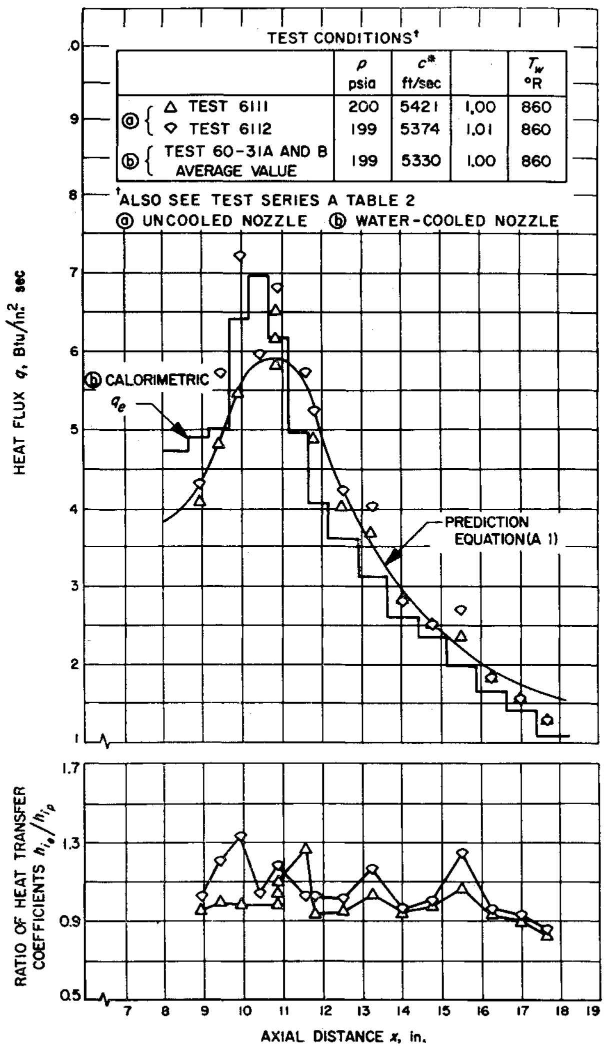

Fig. 4 Heat flux and enthalpy heat transfer coefficient ratio as a function of axial distance for the 1.64-to-1 nozzle at intermediate chamber pressures

For convenience, stagnation enthalpy rather than recovery enthalpy (10) was used to compute the predicted heat flux. Had recovery enthalpy been used, the predicted heat flux would have been reduced approximately 1% in the throat and 7% at the nozzle exit.

Figs. 8–16 show the experimental results in terms of the Stanton, Prandtl, and Reynolds numbers, usually considered to be the dominant variables in convective heat transfer. Fig. 8 shows results for the 2.5-to-1 nozzle at chamber pressures of 208 and 301 psia, in which the Reynolds number variation is caused primarily by the change of local diameter along the nozzle. The flow is treated as being one-dimensional; consequently, the maximum Reynolds number is represented at the throat. If two-dimensional effects had been taken into account, the maximum Reynolds number, based on the static pressure at the wall, would have been found to occur somewhat upstream of the throat. The straight line appearing in all of these figures represents Eq. [1], in which the constant $C = 0.026$. The freestream value of the Prandtl number was calculated from the Euken approximation (11) to be nearly 0.82 for all the tests. The changing shapes of the experimental curves in Fig. 8 are a consequence of the fact that the rate of change of Stanton number with chamber pressure is different at different axial locations in the nozzle. To demonstrate this fact, the experimental Stanton number is presented in Figs. 9–16 as a function of the one-dimensional Reynolds number at given values of area ratio for the 1.64-to-1 uncooled and 2.5-to-1 water-cooled nozzles of Fig. 1 and also the 4-to-1 and 8-to-1 nozzles of Refs. 3 and 4. Figs. 9–12 present the results of the subsonic portions of the four nozzles, whereas Figs. 13–16 show results in the supersonic portions of the same nozzles. In these figures, the increase in Reynolds number is caused by a change in chamber

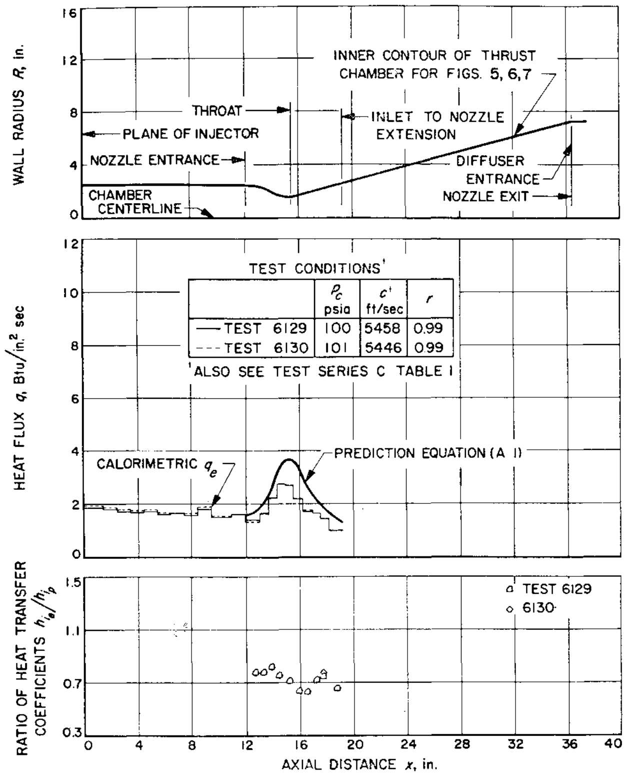

Fig. 5 Nozzle contour, heat flux, and enthalpy heat transfer coefficient ratio as a function of axial distance for the 2.5-to-1 nozzle at low chamber pressures

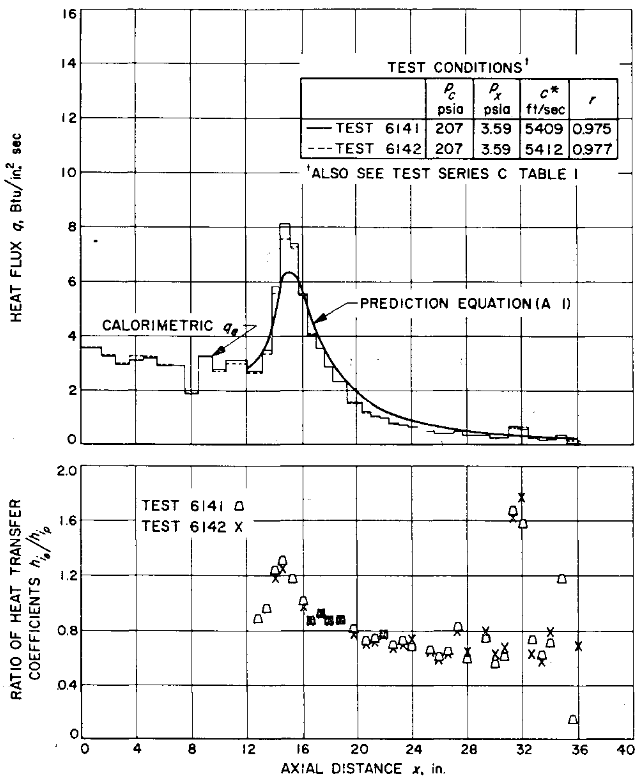

Fig. 6 Heat flux and enthalpy heat transfer coefficient ratio as a function of axial distance for the 2.5-to-1 nozzle at intermediate chamber pressures

pressure. The method used for calculating the Stanton and Reynolds numbers is explained in the Appendix. The results of the uncooled tests, determined by the transient technique for the 1.64-to-1 nozzle, are presented in Figs. 9 and 13 at a wall temperature of 1360°R. This relatively high temperature was chosen in order to avoid the oscillations inherent in the computer solution at lower wall temperatures (see Fig. 2). Because of space limitations of this paper, not all experimental results at intermediate area ratio positions to those shown in Figs. 9–16 could be included; however, all results are given in Ref. 5. For all cases in which significant differences in slope or magnitude of the results exist between the positions shown, the results obtained at intermediate positions exhibited smooth transitions.

The notable trend in the subsonic portion of the nozzles is the progressive increase in the slope of the experimental curves along the flow direction up to but not including the throat in all nozzles. Eq. [1] predicts an increase of heat flux with mass flux to the 0.8 power. However, the experimental results indicate that, for the test conditions, this power is generally too large in the entrance region and too small in the throat region. It is possible that these trends were caused by the particular injector used for all tests. However, the 8-to-1 nozzle was tested with chamber lengths of 3 and 6 in., whereas the 4-to-1 nozzle was tested with chamber lengths of 4 and 8 in. over the same range of pressures, and the trend discussed previously remained equally evident. Either the effects of the injection and combustion processes were not sufficiently damped out by the increases in chamber length to affect the trends, or these trends resulted from other factors not taken into account. The slopes of the experimental curves appear to be nearly constant at large subsonic area ratios. Some of the results at small subsonic area ratios, however, appear to have a variable slope.

The results in the supersonic regions shown in Figs. 13–16 exhibit a trend similar to the subsonic results, in that the slopes of the experimental curves have maxima near the throat and decrease with increasing area ratio, that is, in the flow direction. The results, however, do not appear to have a constant slope at a given area ratio as they do in most of the subsonic region.

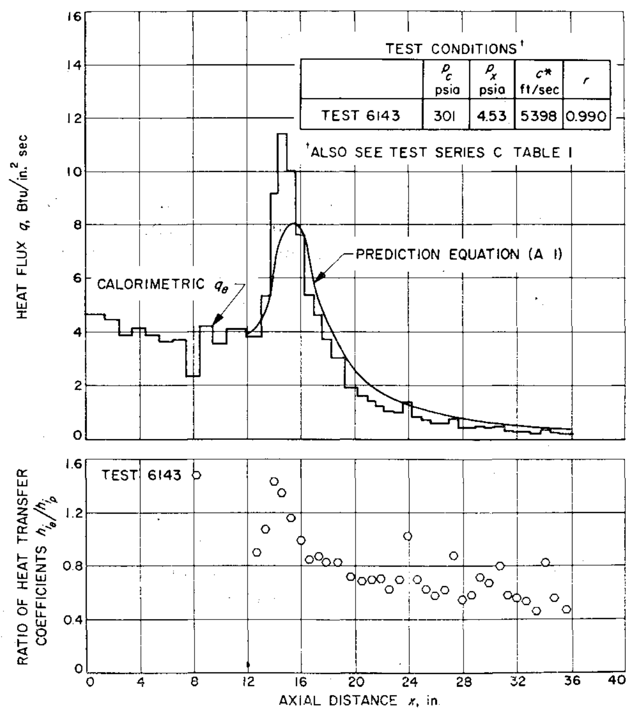

Fig. 7 Heat flux and enthalpy heat transfer coefficient ratio as a function of axial distance for the 2.5-to-1 nozzle at a high chamber pressure

Table 1 Engine components and operating conditions

Test series	p_c, psia	c^*, fps	r	L^*, in.	Injector type	Δp_{IO}	Δp_{SP}	L_c, in.	D_c, in.	ϵ_c	D^*, in.	ϵ_e	Number of tests
A	97 to 246	5300 5379	0.983	17	8-pair Enzian	$0.5p_c$	$0.30p_c$	8	5.00	1.64 to 1	3.90	3.78 to 1	13
B	97 to 246	5269 5173	0.977 0.988	18	8-pair Enzian	$0.5p_c$	$0.23p_c$	5	5.00	2.5 to 1	3.160	2.5 to 1[a]	8
C	100 to 301	5458 5398	0.990 0.990	36	8-pair Enzian	$0.5p_c$	$0.23p_c$	12	5.00	2.5 to 1	3.160	2.5 to 1[a]	9

[a] At chamber pressures above 150 psia, ϵ_e = 20 to 1; that is, the water-cooled extension was attached to the nozzle for these tests.

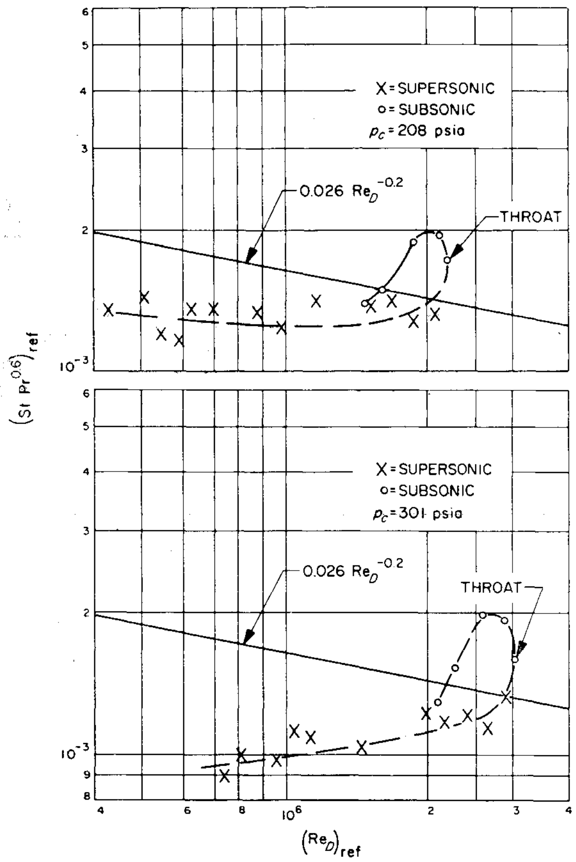

Fig. 8 Stanton number-Reynolds number results for the 2.5-to-1 nozzle at chamber pressures of 208 and 301 psia; Pr = 0.82, L = 35.8 in.

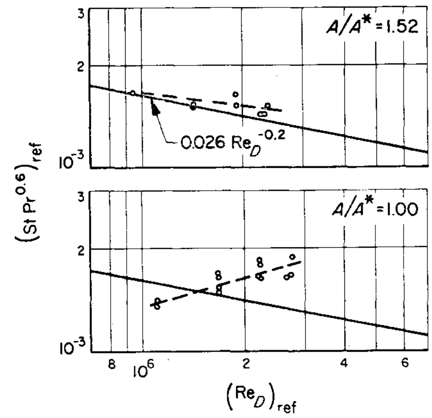

Fig. 9 Stanton number-Reynolds number results at given values of subsonic area ratio for the 1.64-to-1 nozzle; Pr = 0.82, L^* = 17 in.

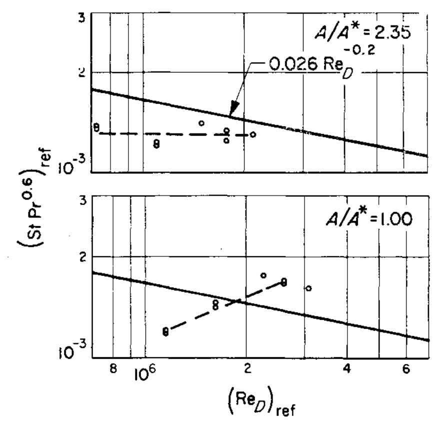

Fig. 10 Stanton number-Reynolds number results at given values of subsonic area ratio for the 2.5-to-1 nozzle; Pr = 0.82, L^* = 35.8 in.

Before attempting to explain the experimental results, it was considered necessary to determine the comparative effect on the Stanton and Reynolds numbers of the one-dimensional mass flow per unit area $(\rho u)_{1\text{-}D}$ and the local $(\rho u)_E$, where $(\rho u)_E$ is defined at the freestream edge of the boundary layer and arises because of the two-dimensional nature of the flow in an axisymmetric nozzle.

The local values of $(\rho u)_E$ for the 1.64-to-1 nozzle were determined experimentally in a smaller but geometrically similar nozzle using air at approximately 60°F and stagnation pressures between 40 and 78 psia. This provided the same range of Reynolds numbers encountered in the rocket tests, but there was essentially no heat transfer. Static-pressure measurements were made axially along the nozzle wall, and density and velocity were calculated using the isentropic flow relation and the perfect-gas equation of state without reference to the area ratios at which the pressure measurements were made. It was assumed that static pressure does not vary across the boundary layer, which was thin compared to the nozzle radius. In Fig. 17, the ratio of $(\rho u)_E$ to $(\rho u)_{1\text{-}D}$ is plotted as a function of area ratio for three flow rates. The three curves are identified by the Reynolds numbers at the nozzle throat. The ρu ratio essentially was found to be independent of Reynolds number at any given area ratio. This means that the effect of using $(\rho u)_E$ in the Stanton and Reynolds numbers (Figs. 9–16) would be a translation of the results with respect to the coordinate axes but not a change of slope at a given area ratio. Thus, the trends discussed previously remain essentially unaffected by the substitution of $(\rho u)_E$ for $(\rho u)_{1\text{-}D}$. The shape of the Stanton number-Reynolds number curve along the nozzle, shown in Fig. 8, would be affected by such a substitution, but most of the points on the curve would be changed by less than 10%, shifting the curves up and to the left when $(\rho u)_E/(\rho u)_{1\text{-}D} < 1$ and down and to the right when $(\rho u)_E/(\rho u)_{1\text{-}D} > 1$.

The differences between Eq. [1] and the experimental results, in particular the rate of change of Stanton number with Reynolds number at a given area ratio, were believed to be either characteristic of the injector used or due to the large favorable pressure gradients that prevailed during the tests. Eq. [1] is based on Reynolds analogy and experimental values of skin-friction coefficient obtained in the absence of a pres-

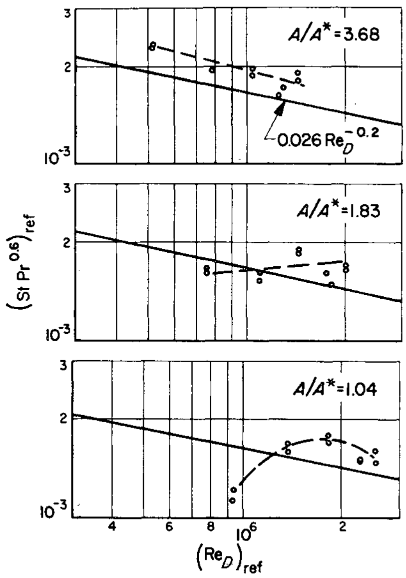

Fig. 11 Stanton number-Reynolds number results at given values of subsonic area ratio for the 4-to-1 nozzle; $Pr = 0.82$, $L^* = 24$ in.

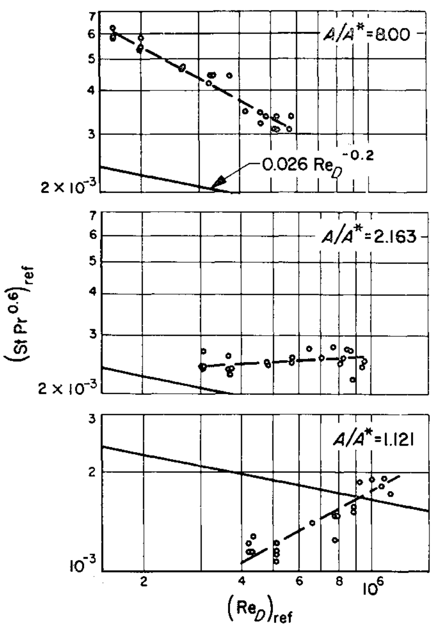

Fig. 12 Stanton number-Reynolds number results at given values of subsonic area ratio for the 8-to-1 nozzle; $Pr = 0.82$, $L^* = 63$ in.

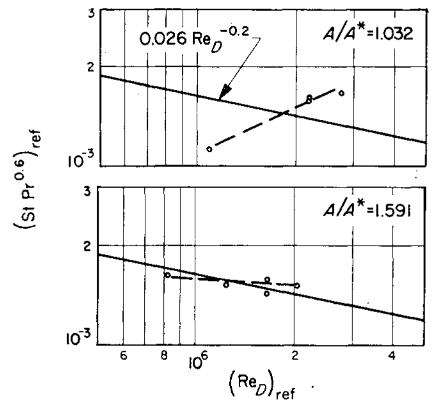

Fig. 13 Stanton number-Reynolds number results at given values of supersonic area ratio for the 1.64-to-1 nozzle; $Pr = 0.82$, $L^* = 17$ in.

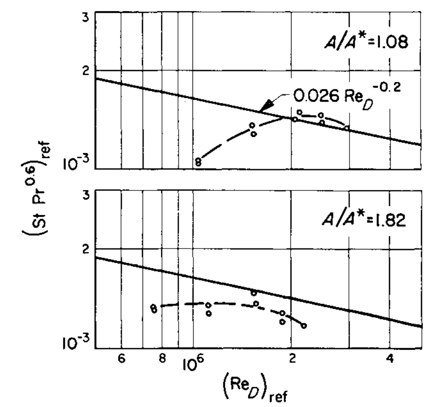

Fig. 14 Stanton number-Reynolds number results at given values of supersonic area ratio for the 2.5-to-1 nozzle; $Pr = 0.82$, $L^* = 35.8$ in.

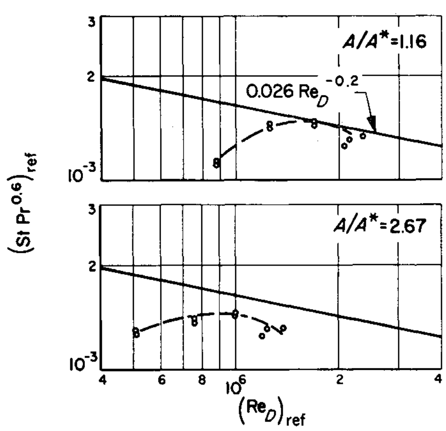

Fig. 15 Stanton number-Reynolds number results at given values of supersonic area ratio for the 4-to-1 nozzle; $Pr = 0.82$, $L^* = 24$ in.

sure gradient. The greatest differences between Eq. [1] and the experimental results occurred near the nozzle throat, where the pressure gradient varied between 75 and 225 lbf/in.^{2}/in. of length. This suggests that large favorable pressure gradients may invalidate Reynolds analogy or that such gradients affect the skin friction coefficient.

A nozzle heat transfer study that is free from injection and combustion effects and that has as an objective the determination of the pressure gradient effect on convective heat transfer is currently in progress at the Jet Propulsion Laboratory (12). The limited results obtained so far indicate that pressure gradient may be an important variable in purely convective heat transfer beyond those predicted by boundary layer development.

As a consequence of the suggested effect of pressure gradient, the general agreement with Eq. [1] and the experimental results, shown in Figs. 3–7, cannot be regarded as confirmation of the equation. Figs. 9–16 indicate that this relatively good agreement may be due to the test conditions, particularly the range of chamber pressures.

Conclusions

Evaluation of the experimental results derived from this investigation and the study of Refs. 3 and 4 have established the following conclusions:

1) In the subsonic region, nozzle heat-flux levels are generally higher and, in the supersonic region, more nearly equal to or somewhat lower than values predicted by a relation similar to the turbulent pipe-flow equation. The heat fluxes in the expansion region from area ratios 4:1 to 20:1

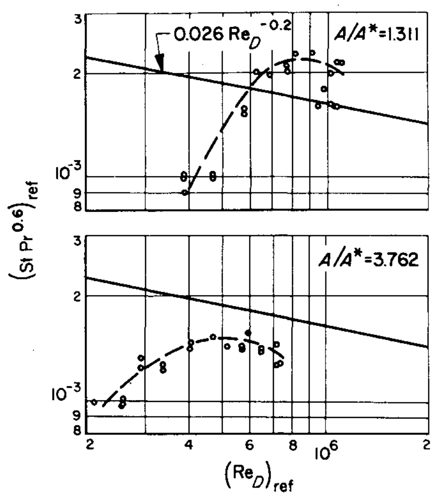

Fig. 16 Stanton number-Reynolds number results at given values of supersonic area ratio for the 8-to-1 nozzle; $Pr = 0.82$, $L^* = 63$ in.

were lower than the predicted values throughout the chamber-pressure range investigated.

2) Heat fluxes substantially higher than predicted are encountered just upstream of the throat. Deviations appear to be related to the chamber pressure, which suggests that pressure gradient may be an important variable in convective nozzle heat transfer with greater influence than predicted by boundary layer development.

3) There are similar trends in the subsonic regions of the two nozzles investigated and those of Refs. 3 and 4. When Stanton number-Reynolds number relationships are considered at fixed locations in a nozzle, allowing Reynolds number to change as a result of varying chamber pressure, the slopes of the experimental curves change progressively from the nozzle inlet to a region just upstream of the throat. Furthermore, the heat-transfer coefficient does not vary with mass flux to the 0.8 power in this region, as predicted by the convective turbulent pipe-flow equation but rather to a smaller power. In the throat region, a power larger than the 0.8 power appears to be required. In the supersonic region, however, the experimental curves do not appear to be straight lines on log-log coordinates as they are in the subsonic region.

4) For the curves discussed in item 3, it was found that substitution of local two-dimensional $(\rho u)_E$ for one-dimensional $(\rho u)_{1\text{-}D}$ resulted in a translation of the curves with respect to the coordinate axes which affected the values of Stanton and Reynolds numbers by less than 10%. However, the slopes of the Stanton number-Reynolds number curves at given area ratios were not influenced by two-dimensional effects.

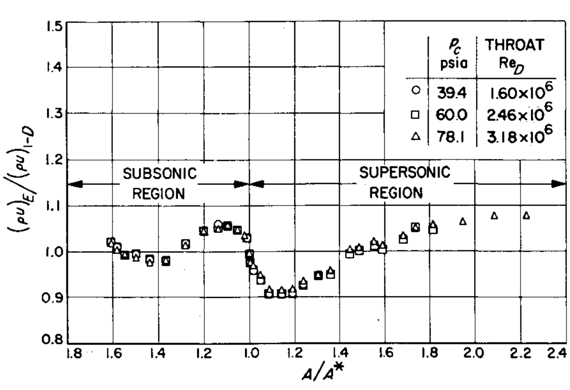

Fig. 17 Ratio of local to one-dimensional mass flow per unit area as a function of area ratio for the 1.64-to-1 nozzle

5) The transient wall-temperature technique of determining local heat fluxes in an uncooled nozzle was found to be reliable, and the results were in agreement with those of the calorimetric technique.

Appendix

The prediction for the heat transfer coefficient in rocket engines developed by Bartz (2) is given as

$$h_{T_p} = \left[\frac{0.026}{(D^*)^{0.2}}\left(\frac{\mu^{0.2}C_p}{Pr^{0.6}}\right)\left(\frac{p_c g_c}{c^*}\right)^{0.8}\left(\frac{D^*}{b^*}\right)^{0.1}\right]\left(\frac{A^*}{A}\right)^{0.9}\sigma \quad \text{[A1]}$$

At given test conditions, only area ratio and σ affect h. The parameter σ accounts for property variations across the boundary layer, caused by temperature variations. It is expressed as

$$\sigma \equiv (\rho_{\text{ref}}/\rho_s)^{0.8}(\mu_{\text{ref}}/\mu_0)^{0.2} \quad \text{[A2]}$$

An expression for the reference temperature is given below.

In Ref. 13, it was suggested that the effect of chemical reaction across the turbulent boundary layer could be accounted for by combining the nonreactive enthalpy heat transfer coefficient, defined as

$$h_i \equiv h_T/\bar{c}_p \quad \text{[A3]}$$

with the reactive enthalpy driving potential as

$$q = h_i(i_0' - i_w') \quad \text{[A4]}$$

The reactive enthalpy potential developed for rocket nozzle flow in the Appendix of Ref. 3 is used for equilibrium combustion products and no dissociated species at the wall, since it comprises both sensible and chemical enthalpy differences between the freestream and the wall conditions. By employing Eq. [A1], which was used for comparison in the section on experimental results, the enthalpy heat transfer coefficient h_i can be calculated explicitly without assigning a value for $\bar{c}_p$, since $h_i = h_p/c_p$. A nonreactive c_p is assumed in the evaluation of the Prandtl number.

Experimental enthalpy heat transfer coefficient h_{i_e} was calculated by Eq. [A4] using the measured values of wall heat flux and the experimental value of enthalpy driving potential which, at constant mixture ratio, is a function of c^* and wall temperature only (Appendix of Ref. 3). In the section on experimental results, results of the ratio of experimental to predicted enthalpy heat transfer coefficients h_{i_e}/h_{i_p} are shown for the 1.64-to-1 uncooled nozzle and the 2.5-to-1 water-cooled nozzle. Experimentally, a local comparison of this ratio can be made for the uncooled nozzle, where local q_e is obtained; however, for the 2.5-to-1 nozzle, an average h_{i_p} is obtained over the coolant-passage width. Hence, h_{i_p} should be averaged for a meaningful comparison. It was found that h_{i_p} based on the average area ratio across the width of a coolant passage provided a good approximation to the average h_{i_p} calculated by use of Eq. [A1]. An average h_{i_p} was calculated for all water-cooled nozzle tests in this manner using the average area ratio.

The Stanton number used in the section on experimental results of the text was defined for chemically reacting flows as

$$St \equiv \frac{q_e/(i_0' - i_w')}{(\rho_{\text{ref}}u)_{1\text{-}D}}$$

By using the definition of h_i in Eq. [A3],

$$St = h_i/(\rho_{\text{ref}}u)_{1\text{-}D} \quad \text{[A5]}$$

where ρ_{ref} is the gas density evaluated at the reference temperature. The reference temperature (10) may be computed by

$$T_{\text{ref}} = 0.5(T_s + T_w) + 0.22\, Pr^{1/3}\,(T_0 - T_s) \quad \text{[A6]}$$

The Prandtl number $Pr = 0.82$, which, for the given test conditions, may be assumed a constant.

Reynolds number is given as

$$Re_{D\mathrm{ref}} = (\rho_{\mathrm{ref}} u D/\mu_{\mathrm{ref}})_{1-D}$$

where μ, the dynamic viscosity, was estimated by

$$\mu = 2.54\ (10^{-8}) \times T(0.6_{\mathrm{ref}})\ \mathrm{lbm/sec\text{-}in.}$$

for diatomic molecules (14). For the water-cooled nozzles, average heat flux is obtained, and D, T_{ref}, u, etc., are based on the average area ratio between coolant-passage ribs.

Acknowledgment

The authors wish to express their appreciation for the assistance rendered by Claude D. Pearce and John A. MacKay, who operated the experimental equipment; Harold L. Gier, who obtained the data and calculated results shown in Fig. 17; Paul H. Steinbrook, who assisted with most of the calculations; and Paul F. Massier, who offered many helpful suggestions.

References

1 Bartz, D. R., "An approximate solution of compressible turbulent boundary layer development and convective heat transfer in convergent-divergent nozzles," Trans. Am. Soc. Mech. Engrs., 1235–1245 (November 1955).

2 Bartz, D. R., "A simple equation for rapid estimation of rocket nozzle convective heat transfer coefficients," Jet Propulsion **21**, 49–51 (1957).

3 Welsh, W. E., Jr. and Witte, A. B., "A comparison of analytical and experimental local heat fluxes in liquid-propellant rocket thrust chambers," Jet Propulsion Lab. TR 32-43, Pasadena, Calif. (February 1, 1961).

4 Welsh, W. E., Jr. and Witte, A. B., "A comparison of analytical and experimental local heat fluxes in liquid-propellant rocket thrust chambers," Trans. Am. Soc. Mech. Engrs., 19–27 (February 1962).

5 Witte, A. B. and Harper, E. Y., "Experimental investigation and empirical correlation of local heat-transfer rates in rocket-engine thrust chambers," Jet Propulsion Lab. TR 32-244, Pasadena, Calif. (March 19, 1962).

6 Massier, P. F. and Roschke, E. J., "Experimental investigation of exhaust diffusers for rocket engines," *Progress in Astronautics and Rocketry: Liquid Rockets and Propellants* (Academic Press, New York, 1960), Vol. 2, pp. 3–75.

7 Powell, W. B., Howell, G. W., and Irving, J. P., "A method for the determination of local transient heat flux in uncooled rocket motors," Jet Propulsion Lab. TR 32-257, Pasadena, Calif. (July 1, 1962).

8 Elverum, G. W., Jr., Martinez, J. S., and Gillespie, R. W., "Results of theoretical rocket motor performance calculations for liquid propellant systems," Jet Propulsion Lab. Memo. 20-159, Pasadena, Calif. (November 1, 1957).

9 Green, L., Jr., "Flow separation in rocket nozzles," ARS J. **23**, 34–35 (1953).

10 Eckert, R. G., "Survey on heat transfer at high speeds," Wright Air Dev. Center TR 54-70 (April 1954).

11 Bartz, D. R., "The role of transport properties in problems of jet engines and rockets," *Transport Properties in Gases, Proceedings of the Second Biennial Gas Dynamics Symposium* (Northwestern Univ. Press, Evanston, Ill., 1958), pp. 105–118.

12 Witte, A. B., and Harper, E. Y., "Heat transfer in rocket motors," Jet Propulsion Lab. Research Summary 36-11, Pasadena, Calif., pp. 80–85 (November 1, 1961).

13 Bartz, D. R., "Six-part survey-rocket heat-transfer literature; predictions of thermal properties," Trans. Am. Soc. Mech. Engrs., 162–166 (August 1960).

14 Hilsenrath, J., Beckett, C., Benedict, W., Fano, L., Hoge, H., Masi, J., Nuttall, R., Touloukian, Y., and Woolley, H., "NBS-NACA tables of thermal properties of gases," Natl. Bur. Standards Circular 564 (1955).